Acta Oceanol. Sin., 2019, Vol. 38, No. 2, P. 1–10
https://doi.org/10.1007/s13131-018-1163-y
http://www.hyxb.org.cn
E-mail: hyxbe@263.net

Flow modification associated with mangrove trees in a macro-tidal flat, southern China

Yang Chang[1], Yining Chen[1, 2*], Yan Li[1, 2]

[1] Second Institute of Oceanography, Ministry of Natural Resources, Hangzhou 310012, China

[2] State Key Laboratory of Marine and Environmental Science, Xiamen University, Xiamen 361005, China

Received 17 September 2017; accepted 10 November 2017

Abstract

Limited studies have investigated the modification of tidal currents by mangrove trees. In particular, the impacts of mangrove trees on a vertical velocity profile remain unclear. An automatic system is developed to observe the vertical velocity profiles within a mangrove forest composed of artificially introduced *Kandelia obovata* located on the Ximen Island, the southern Zhejiang Province. The results reveal low flow velocities throughout the vertical profile within the mangrove forest. The vertical profile shows an overall decrease of the velocity with an increasing height above the bed. This pattern is due to the vertical increase of the drag force by the trunks and tree canopies. In addition, the turbulent energy density also varies vertically, corresponding to the vertical structure of the mangrove trees. In comparison with the vertical structure of flows within bare mudflats (semi-logarithmic) and salt marshes (nearly J-shape), the mangrove trees are shown to have a considerable impact on the vertical velocity profile in different ways.

Key words: mangrove trees, flow, energy dissipation, vertical structure

Citation: Chang Yang, Chen Yining, Li Yan. 2019. Flow modification associated with mangrove trees in a macro-tidal flat, southern China. Acta Oceanologica Sinica, 38(2): 1–10, doi: 10.1007/s13131-018-1163-y

1 Introduction

Coastal wetlands are an important buffer zone of the global environmental change because they can modify currents, damp waves, promote sediment deposition and provide habitats for coastal organisms (Perillo et al., 2009; Barbier et al., 2011). There are three primary types of coastal wetlands in the world: mangrove swamps, salt marshes and seagrass beds. Coastal wetland plants are widespread and cover the intertidal and subtidal zones. The intertidal zone mainly includes mangrove trees and salt marshes, whereas sea grass beds can extend to the subtidal zone. Coastal wetland plants are affected by the forces of waves and currents, which form the physical settings of the plants' growth environment. The plants in the intertidal zone can often change the dynamic conditions of waves and flows to create environments beneficial for their own survival (Mitsch and Gosselink, 2000).

Intertidal plants affect flow via complex processes. From a spatial perspective, plants can impact the horizontal and vertical velocity profiles. From an energy perspective, plants can affect the low-frequency energy (mean flow) and high-frequency turbulent energy of the flow. As shown by the characteristics of the vertical velocity profile, the flow structure on bare flats (plant-free) is consistent with the theory of a turbulent boundary layer (Soulsby, 1997). When the seabed is considered to be a smooth wall, a standard boundary layer exists that consists of a very thin (a few millimeters thick) viscous sublayer close to the wall and a transition layer (buffer layer) directly over it. The fully turbulent logarithmic layer is located above the transition layer (Middleton and Southard, 1984). However, when herbaceous plants are present on the tidal flat, the features of the bottom boundary layer will vary. Compared with the standard boundary layer, the presence of salt marsh plants increases the roughness and changes the structure of the vertical velocity profile (Leonard and Luther, 1995; Leonard and Croft, 2006). Field observations have indicated that when the plant canopy is not completely submerged, the vertical velocity profile follows a semi-logarithmic distribution. However, when the canopy is completely submerged, an obvious transition layer appears in the top part of the canopy due to the differences of the flow structure in and above the canopy (Neumeier and Amos, 2006). Shi et al. (1996) used a laboratory flume to observe the flow velocity profile at different relative water depths within a *Spartina anglica* canopy and found that the flow structure in the plants has three main hierarchical layers, including the layer at the bottom of the canopy, the transition layer, and the layer in the upper part of the canopy. Above the canopy, the vertical velocity profile follows a semi-logarithmic distribution and exhibits a J-shape. The flow velocity inside the canopy exhibits a reverse gradient, and the overall vertical velocity profile has an S-shape. Because the vertical biotic characteristics of mangrove trees vary considerably, the characteristics of the velocity profile of the bottom boundary layer may exhibit the opposite pattern to that of the plant canopy of salt marshes.

Previous studies on the structure and intensity of turbulence have found that the turbulent energy inside the plant canopy of salt marshes (such as the canopy of *Spartina alterniflora*) be-

Foundation item: The National Natural Science Foundation of China under contract Nos 41006047 and 41776096; the Fundamental Research Fund of the Second Institute of Oceanography, State Oceanic Administration of China under contract No. JT1505.
*Corresponding author, E-mail: yiningchen5410@hotmail.com

comes consistent in the vertical direction, whereas the turbulence of the water above the canopy is not affected by the plant. The turbulent energy increases rapidly from the bottom to the top and is dependent on the plant structure (Neumeier and Amos, 2006). Several studies have proposed that plants decrease the relatively large turbulence length on the bare flats by changing the turbulence length (associated with the plant characteristics), which dissipates the turbulent energy (Nepf, 2012). Owing to the unique biophysiological characteristics of mangroves, such as their networks of trunks and their aerial roots, the energy dissipation caused by mangroves is very complicated and is associated with the generation of eddies and wakes (Massel et al., 1999; Mazda and Wolanski, 2009). A recent study of mangrove trees and salt marshes in Yunxiao in southern Fujian Province (Chen et al., 2016) showed that the turbulent energy could be reduced by more than 86% in both mangrove trees and salt marshes compared with bare mudflats. The relative dissipation efficiency of the turbulent energy for the two types of plants depends on the relative water level. When the water level is below the canopy of the mangrove trees, the energy dissipation ability is relatively low; when the water level reaches the canopy of the mangrove trees, the energy dissipation ability increases and becomes more effective than that of salt marshes.

From the perspective of coastal protection, previous studies have focused on the influence of mangrove swamps on waves. Unlike salt marsh grasses, the canopies of mangrove trees are generally elevated above the seabed with trunks and aerial roots (pneumatophores) beneath. The wave dissipation ability of mangrove trees may therefore depend greatly on the vegetation structure and the relative submersion depth (Massel et al., 1999; Quartel et al., 2007; Bao, 2011).

Mangrove plants are woody, with the upper part featuring a flexible canopy and the lower part of a rigid trunk. The aerial roots are the roots that develop above the bed, and they have different forms depending on the species. Mangrove plants have many differences in morphology compared with the herb plants of salt marshes and seagrass beds. The vertical features of the canopies of mangrove trees, which are the focus of research on hydrodynamic forces, are more complicated than those of salt marshes and sea grasses. However, there are no detailed reports on the vertical velocity profile associated with mangrove trees. Therefore, the observations and studies of the vertical velocity profile of mangrove trees have scientific significance and application value.

Selecting a typical coastal region of mangrove swamps in China to conduct field observations, we obtained the records of the vertical profile features of flows and the turbulence due to the effects of mangroves. On the basis of the features of the vertical velocity profile, the turbulence intensity and spectrum characteristics, we interpreted the modulating action of the mangroves on the tidal flow.

2 Study area

The research site is located in the special marine reserve area (28°20′55.93″N, 121°10′45.48″E) of the Ximen Island in Zhejiang Province. It is located on the northern side of the Yueqing Bay on the southeastern coast of China (Fig. 1a), where is affected by strong irregular semidiurnal tides. The tidal range is relatively large with a mean tidal range of 5.15 m, and the maximum tidal range can reach 8.34 m in the bay. The flow in the bay is a reciprocating flow, and the mean flow velocities of the flooding and ebbing spring tides in the entire bay are 17–73 and 40–84 cm/s, respectively, which are more than three times faster than the neap tides. The flow velocity during the ebbing tides is generally greater than that during the flooding tides (Han and Yang, 2017). The flow velocity at different topographic positions differs considerably; the flow velocity is relatively slow in the inner bay, the average vertical flow velocity is 40 cm/s in the water channel, and it is less than 20 cm/s in the lower part of the tidal flat. The flow velocity of the flooding tides near the sea area of the Ximen Island averages 59 cm/s, and the flow velocity of the ebbing tides averages 63 cm/s (Han and Yang, 2017). The Yueqing Bay is a

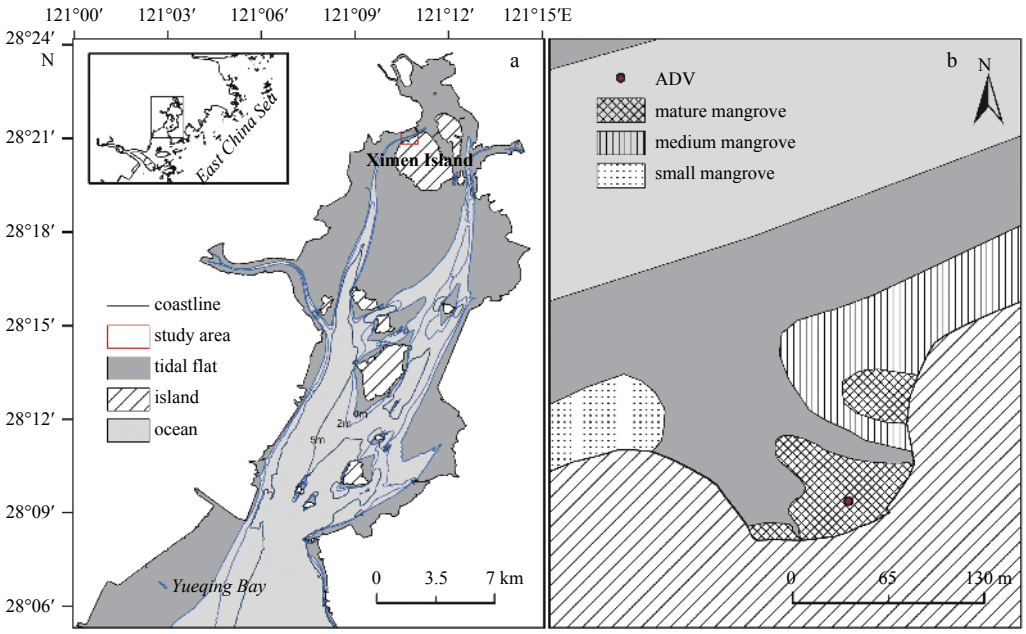

Fig. 1. Location of the study area and the observation setup: regional map of the Ximen Island (a), and vegetation distribution map and the location of the ADV deployments (b). The mangrove classification (small, medium and mature) was based on the age of planting.

long and narrow semi-enclosed bay, and the Ximen Island is located at the head of the bay. Except for during extreme weather conditions, the effect of waves is insignificant because the bay is shielded by the island (one to two typhoons affect this area each year); therefore, the hydrodynamic force is caused mainly by tidal currents (Han and Yang, 2017).

The special marine reserve area of the Ximen Island in Zhejiang Province (Fig. 1) is the northernmost region for successful artificial planting of mangrove trees in China, and it has special geographical significance. Currently, the total area of mangrove trees in the protected zone is 7.9 hm^2. Most of the mangrove trees were planted over the last few decades and have formed short and medium height mangroves. However, there is a mature mangrove zone that was planted 60 a ago in the northwestern part of the island (Fig. 1b), and this area was selected for this study. The mangrove plants are monotypic *Kandelia candel* with a high canopy closure, and the average space between the plant trunks is approximately 2 m, which is equivalent to the width of the tree canopy. The aerial root system appears sparsely on the ground and is less than 20 cm high (Han and Yang, 2017). No other plant species were observed on this tidal flat; therefore, this area is suitable for conducting the field observations of the mangrove canopy-hydrodynamic force interaction. Therefore, the mature mangrove zone in the northwest Ximen Island was selected to perform a field plant investigation of mangroves and observations of the hydrodynamic force to examine the influence of the canopy of mangrove trees on the hydrodynamic force.

3 Methods

3.1 *Instrument deployment and operating mode*

This study investigated a single location within the mangroves. To obtain the vertical velocity profile in the mangrove trees, we used a three-dimensional acoustic Doppler velocimeter (ADV) (Nortek Vector, Norway) installed on a mobile frame to obtain single-point measurements at different heights above the bed of mangroves. This ADV can accurately measure the three components of the flow velocity of a sampling volume (using a cylinder with a diameter of approximately 15 mm and a height of 15 mm) at a distance of 15 cm from the probe. The range of the velocity measurements for the instrument was set to between 0 and 0.1 m/s. The measuring accuracy is 0.5% of the measurement value, and the measurement noise of the instrument is less than 1 mm/s. To obtain the profile information of the flow velocity, we developed a stainless steel observation frame (Chinese Patent No. ZL20130278911.6) that can rise and fall according to pre-selected heights once the tidal depth is sufficient. The ADV was carried by the lifting frame to observe the vertical profile. The heights of the fixed point observations are illustrated in Fig. 2a and the heights are relative to the bed of the flat.

The lifting frame is primarily made of non-magnetic stainless steel, which does not cause magnetic interference with the instrument. Electronic parts are watertight and can work under 1–2 m of water. This instrument mainly consists of five parts (Fig. 2b): (1) a support frame; (2) a transmission device that can drive the repetitive up and down motions of the instrument and can re-

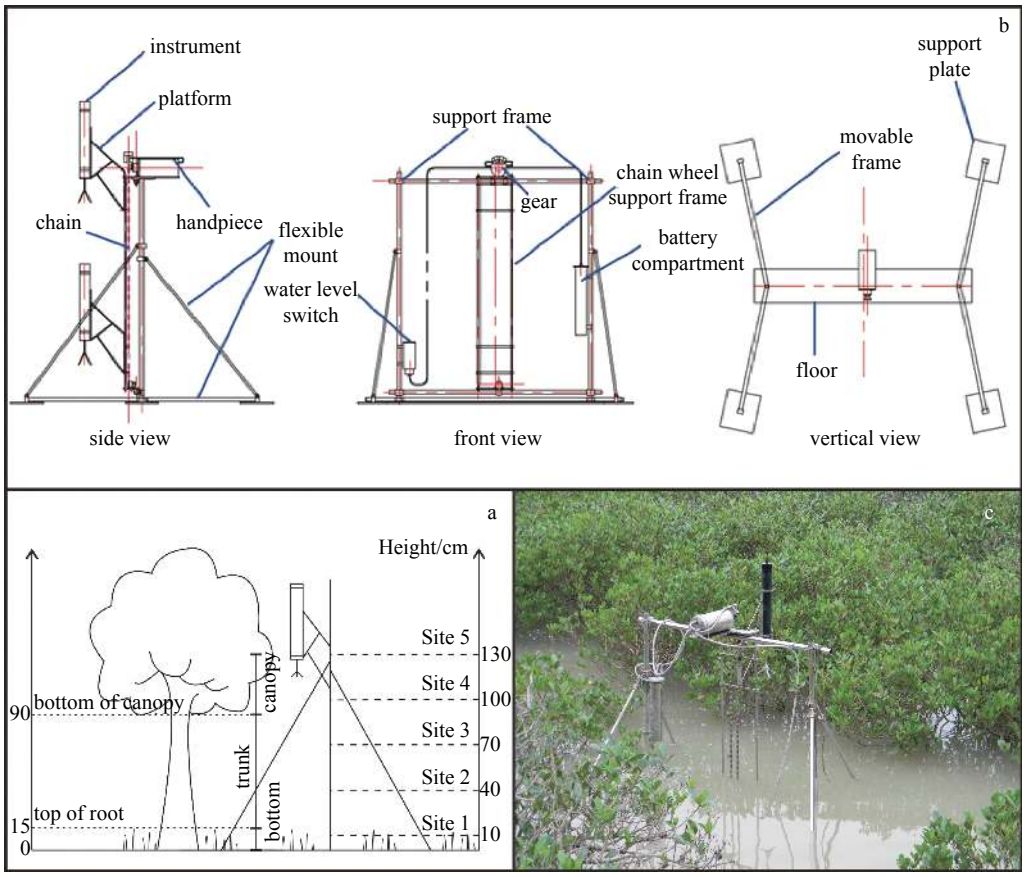

Fig. 2. Vertical distribution of the fixed positions along the vertical profile with reference to the mangrove height, all heights are above the bed of the tidal flat (a); automatic lifting frame: details of the automatic lifting frame (b); and field photo of the automatic lifting frame (c).

main at a series of set heights for 5 min so that the device can complete fixed-point observations at a high frequency; (3) a platform for carrying the devices; (4) a battery compartment; and (5) a water level switch (20 cm from the bottom).

To determine the effect of mangrove plants on the vertical velocity profile, we selected the time period of the spring tides on June 19–20, 2011, to observe the tidal flows. To deploy the automatic lifting system, an area with a low canopy closure was selected so that the frame could fit into the space between the mangrove trees (Fig. 2c). The basic description of the site follows as: The lifting frame was placed at a low elevation bed without mangrove trees, and the distance between the lifting frame and the surrounding plants was approximately 1 m (Fig. 2a). The ADV sensor was positioned less than 50 cm from the adjacent trees, which allowed the measurement of the plants' impact. The biological properties of the vegetation, including the vegetation height, canopy properties and vegetation spacing, were also measured *in situ* using measuring tapes. The bottom of the mangrove canopy was approximately 90 cm higher than the bottom of the lifting frame, the upper part of the canopy was approximately 180 cm high above the bed, and the central region of the canopy (i.e., the part where the leaves are the densest) was approximately 120 cm high above the bed. The ADV repeatedly moved up and down on the lifting frame (Fig. 2a). The observation heights were set at 10, 40, 70, 100 and 130 cm above the bed (same as the bottom of the mangrove trees), and the ADV remained at every height for 5 min while continuously sampling at 16 Hz to obtain three-dimensional data of the flow velocity (Fig. 2a).

It is worth noting that when the water reached the water level switch, the transmission device began to operate, and the instrument performed an observation by moving from the highest position to the lowest position. Because the instrument moved faster than the rate of a water level rise, we only obtained effective data in the middle period of the tidal cycle.

3.2 *Data processing*

The time series of pressure and flow velocity data was output from the ADV, and the pressure data were converted to water level data. On the basis of the water level variation, the time series (5 min) of the flow velocity of each fixed point was extracted. The components of the flow velocity at each fixed point were rotated horizontally based on the main direction of the flow to obtain the velocity components u, v and w, where u is the flow in the main flow direction, v is the flow perpendicular to the main flow direction, and w is the upward flow. Before we calculated the mean velocity at the fixed location, we adopted the phase-space thresholding method developed by Goring and Nikora (2002) to denoise the original data. The water level at the fixed point was converted from the average water depth measured by the ADV pressure probe by adding the height difference between the pressure probe and the ADV measurement point.

Because the vertical movement of the instrument is uniform and slow, except for the data collected at the fixed points, the flow velocity data of the moving segments can be extracted based on the movement pattern of the instrument (each movement segment was 2 min). The horizontal flow velocity components were extracted, and the average value was obtained by rotating the component based on the main direction of the flow to supplement the results of the fixed points.

To analyze the turbulence, the instantaneous flow velocities (u, v, w) can be decomposed into the time-average flow velocities (U, V, W) and the fluctuating velocities (u_t, v_t, w_t), such as u=U+u_t. The turbulence intensities (i_u, i_v, i_w) are defined as the root-mean-square of the fluctuating velocity (Neumeier and Amos, 2006) and are calculated as follows:

$$i_u = \sqrt{\overline{u_t^2}},\ i_v = \sqrt{\overline{v_t^2}},\ i_w = \sqrt{\overline{w_t^2}}, \tag{1}$$

The turbulent kinetic energy (TKE) (Neumeier and Amos, 2006) is calculated as follows:

$$\mathrm{TKE} = \frac{1}{2}\rho\left(\overline{u_t^2} + \overline{v_t^2} + \overline{w_t^2}\right), \tag{2}$$

where ρ is the liquid density. The three-dimensional Reynolds stress τ_{xyz} (Neumeier and Amos, 2006) is calculated as follows:

$$\tau_{xyz} = \rho\left(\overline{u_t v_t}^2 + \overline{v_t w_t}^2\right). \tag{3}$$

In addition, we use an autocorrelation function to calculate the energy spectral density of the three components separately.

4 Results

4.1 *Water level variation*

Although the measurements lasted from the middle to spring tidal cycle, the water only reached the mangrove canopies during the spring tides to form a complete vertical profile record. Thus, we only used the data from June 19–20, 2011, when the spring tides occurred. The water levels are shown in Fig. 3, which includes a nighttime tide (Fig. 3a) and a daytime tide (Fig. 3b). The highest water level during the nighttime tide is approximately 170 cm above the bed, the average water level during the observation is 145 cm, and the average water level during the daytime tide is 80 cm. The difference in the average water level between the two tidal cycles is 65 cm; the water level reaches the canopy of the trees during the nighttime high tide, whereas it fails to submerge the canopy during the daytime high tide. On the basis of the change in the water level and the vertical biological characteristics of the plants, we divide the mangrove trees into three parts: the near-bottom part, which is composed of bare mudflat and sparse aerial roots or long hypocotyls of seedlings (0–15 cm), the trunk layer (15–90 cm) and the canopy (above 90 cm) (Fig. 1c).

4.2 *Vertical velocity profile characteristics*

Figures 3c and d show the horizontal flow velocity at different heights during the nighttime and daytime high tides, respectively, and the fit to the velocity data during the nighttime high tide. The flow velocity is very low over all of the mangroves. During the nighttime high tide, the flow velocity is less than 4 cm/s, and the flow velocity near the bottom is approximately three times that in the canopy. During the daytime high tide, the flow velocity on the bottom is less than 1 cm/s (Table 1). The directions of the flow velocity at different time and at different locations are shown by the arrows in Fig. 3a. The flow direction is essentially consistent beneath the canopy, and there is an apparent deflection in the flow direction within the canopy.

To present the final results, we calculated the average horizontal flow velocity at the fixed points and used the standard deviation as the error to plot the velocity profile (Fig. 4a, Table 1). In the vertical distribution of the flow velocity under the canopy, the flow velocity decreases as the height increases, and the vertical velocity profile exhibits an inverse logarithmic distribution. Near

Table 1. Summary of flow and turbulence properties at three levels (nighttime)

Parameter	Notation and units		Mean value		
			Aerial roots (or hypocotyls) (0–15 cm)	Trunk (15–90 cm)	Canopy (90–130 cm)
Flow velocity	U	m/s	0.025	0.012	0.005
Turbulence intensity	i_u	m/s	0.002 6	0.001 4	0.002 3
	i_v	m/s	0.001 8	0.001 3	0.001 6
	i_w	m/s	0.001 6	0.000 75	0.001 3
Turbulent kinetic energy	TKE	J/m^3	0.006 5	0.002 5	0.005 5
Shear stress	τ_{xy}	N/m^2	1.48×10^{-4}	7.23×10^{-4}	1.91×10^{-3}

Note: The three levels are defined by the biological properties of the mangrove trees: the aerial roots (bottom layer), the trunk and the canopy.

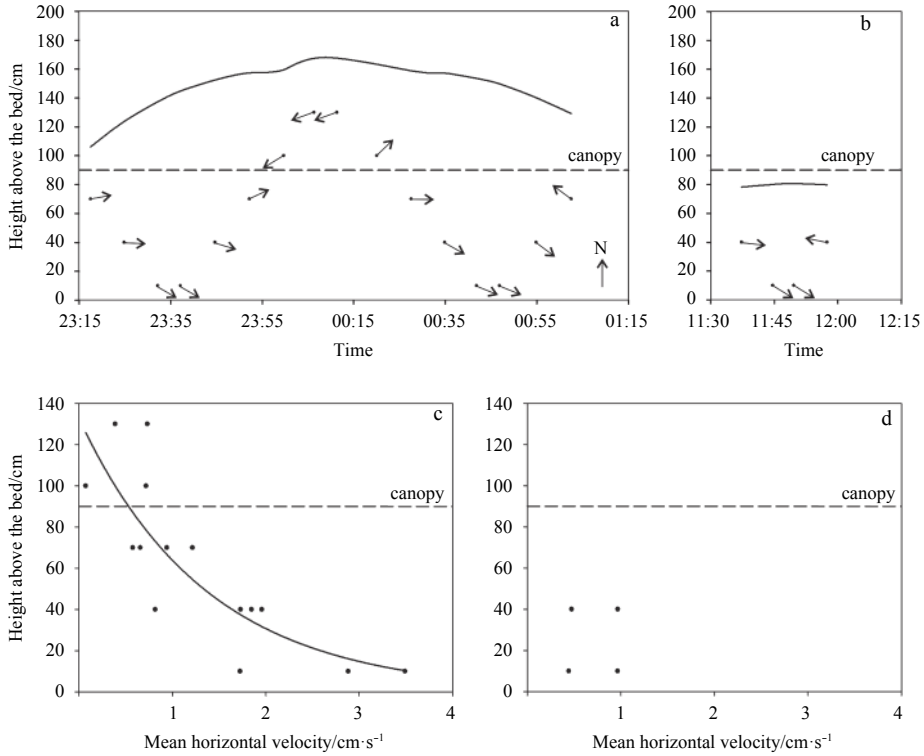

Fig. 3. Water level variations and flow characteristics: water level variations and flow direction variations throughout the measurement period (nighttime), where flow vectors are based on the earth coordinate system at different heights above the bed (a); water level variations and flow direction variations throughout the measurement period (daytime) (b); mean horizontal flow velocity throughout the measurement period (nighttime) (c); and mean horizontal flow velocity throughout the measurement period (daytime) (d).

the bottom, the standard deviation of the flow velocity is relatively large; in the middle trunk layer, the data of the flow velocity tend to converge. On the basis of the average data obtained inside the canopy, which are relatively limited, the flow velocity inside the canopy tends to decrease slightly in comparison with the bottom of the canopy.

To supplement the data of the flow velocity at a fixed point (Fig. 4), the horizontal flow velocities of the moving segments can be joined together to form another set of profiles of the flow velocity due to the limited influence of the slow vertical velocity (30 cm in 2 min) on the horizontal flow velocity, as shown in Fig. 4b. Because the change in the water level is very limited, we can approximate the velocity profile as being measured at the same time. The profile of the flow velocity in the vertical direction after the combination essentially matches the reverse logarithmic distribution. The flow velocity near the canopy is very low (much less than 1 cm/s), and it approaches a consistent flow in the vertical direction. In the trunk part, the horizontal flow velocity decreases linearly with the increasing height. The flow velocity is the highest at the bottom, and the points of the flow velocity are relatively scattered. It is worth noting that a reverse gradient of the flow velocity is sometimes observed at the bottom (Fig. 4b, bottom right corner), which could be caused by the root system at the bottom of the mangroves, resulting in a decrease in the flow velocity near the bottom.

4.3 *Turbulence fluctuation*

4.3.1 *Magnitude of the turbulent energy*

The calculated results of the turbulent energy and the Reynolds stress in different layers within the mangroves are shown in Table 1 and Fig. 5. The turbulence intensity near the canopy is similar to that in the near-bottom layer, which is approximately three times that in the trunk layer. The distribution of the vertical

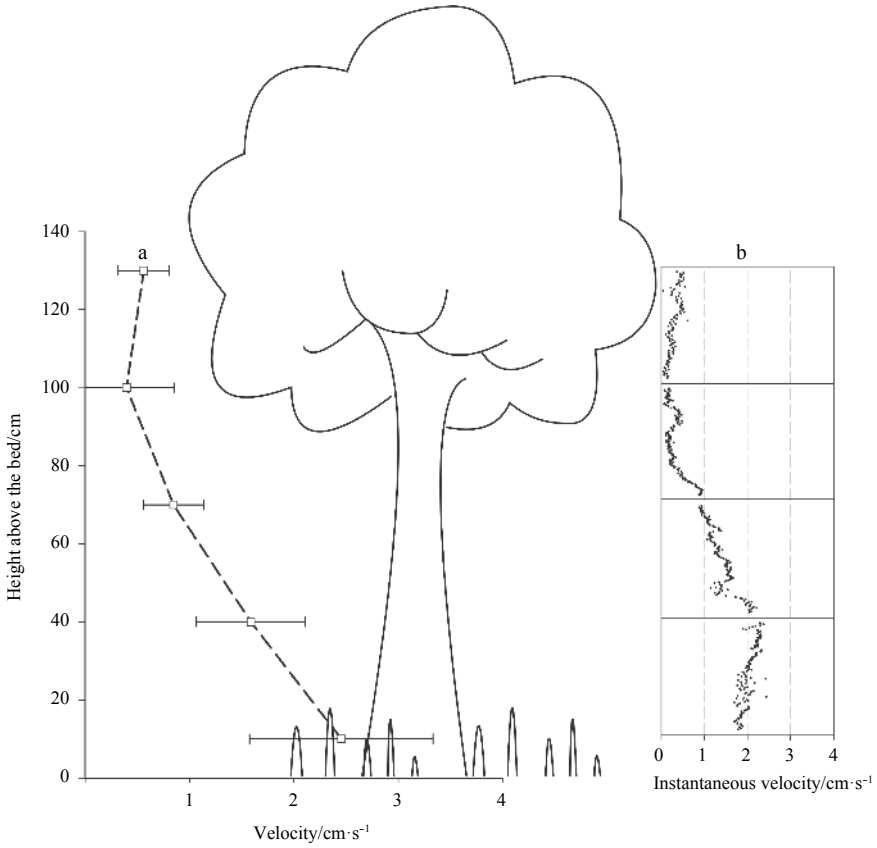

Fig. 4. Vertical profiles of flows: vertical distribution of the mean horizontal flow velocity and standard deviation based on fixed-point observations (a), and vertical distribution of the horizontal flow velocity based on the movement period of the lifting frame (b).

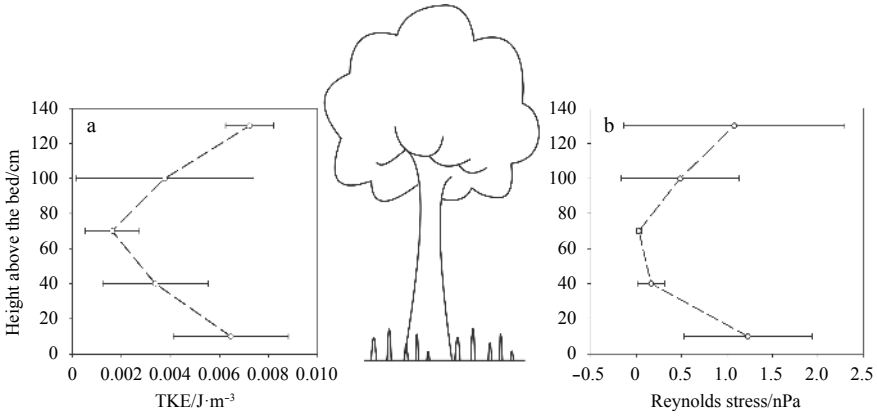

Fig. 5. Vertical distributions of turbulence and stress: TKE (a) and three-dimensional Reynolds stresses (b).

turbulent energy is not uniform within the mangroves; the water turbulence is restrained in the trunk layer, and the vertical distribution of the turbulent energy follows a C-type distribution (Fig. 5a), which indicates that different parts of the mangrove trees have different influences on the flow. The vertical distribution of the Reynolds stress has a similar pattern (Fig. 5b). The stress is high in the near-bottom layer, decreases gradually in the trunk layer, and starts to increase near the canopy, which indicates that the vertical distribution of the drag force caused by different parts of the plants is not uniform. Both the turbulent energy and the Reynolds stress are very small in the range of the mangroves, which is related to the low energy conditions in this region.

4.3.2 *Spectral analysis*

By researching the energy spectra of the flow speed components, we can understand the distribution of the turbulent energy in different frequency bands within the vegetated mudflat. The power spectral curves at different heights within the mangroves during the daytime and nighttime high tides are shown in Figs 6 and 7, respectively.

On the basis of Kolmogorov's scaling law for the turbulent flow, within the inertial subrange, the dissipation process of the turbulent energy is generally consistent with a negative five thirds (–5/3) power law. In this study, when the water level reaches the canopy (Fig. 6) but only approaches the near-bottom part, the energy spectrum between 0.1 and 1.0 Hz essentially matches this

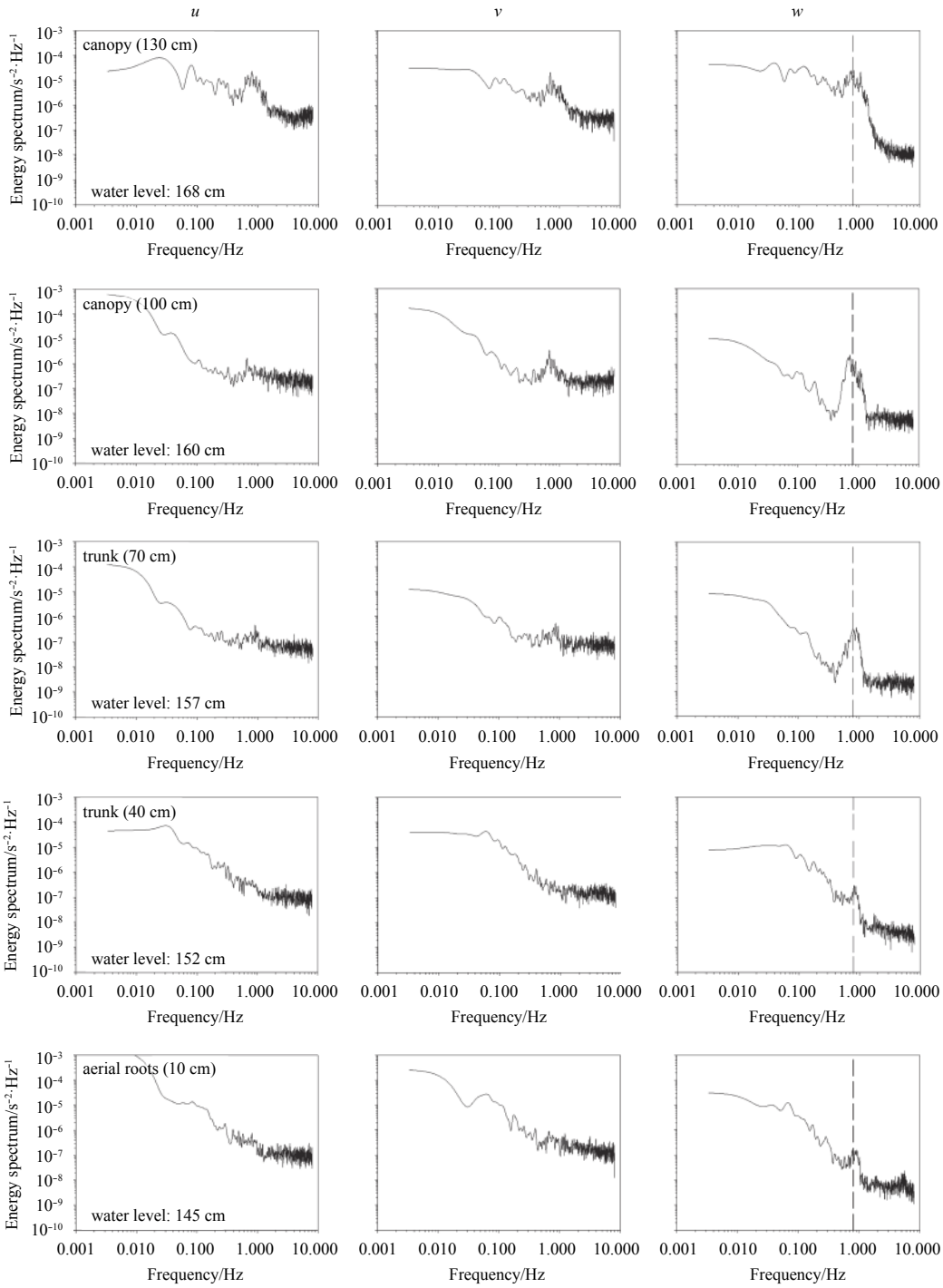

Fig. 6. Energy spectrum plots of the three flow components based on fixed-point measurements at five elevations.

power law, similar to the bare mud flats. Near the trunk and canopy parts, the slope of the energy dissipation becomes small, the energy dissipation is mainly concentrated in the low frequency region (<0.1 Hz), and the high frequency portion of the inertial subrange does not match the power law. This illustrates that the energy dissipated in the canopy is different from that in the near-bottom part. Most of the high-frequency energy are absorbed by the canopy, and the main energy has low frequency features. When the water level fails to reach the canopy, a pattern similar to that of the trunk layer appears in the near-bottom layer (Fig. 7).

It should be noted that there is a region of peak values at approximately 0.8 Hz in the energy spectrum of the theoretical flow velocity (dotted lines in Fig. 6). The greater the distance to the ground, the larger the peak value. We also find similar patterns for the power spectral curves in the horizontal direction in parts of the canopy and the trunk layer, but the peak values are relatively small. This indicates that there is a relatively strong band of energy storage at approximately 0.8 Hz within the mangroves. On the basis of the average water depth, the propagation velocity of the tidal wave is estimated to be 3.6 cm/s $\left(\sqrt{gh},\ h=1.3\ \text{m}\right)$, the wavelength corresponding to 0.8 Hz is approximately 4.5 m, and

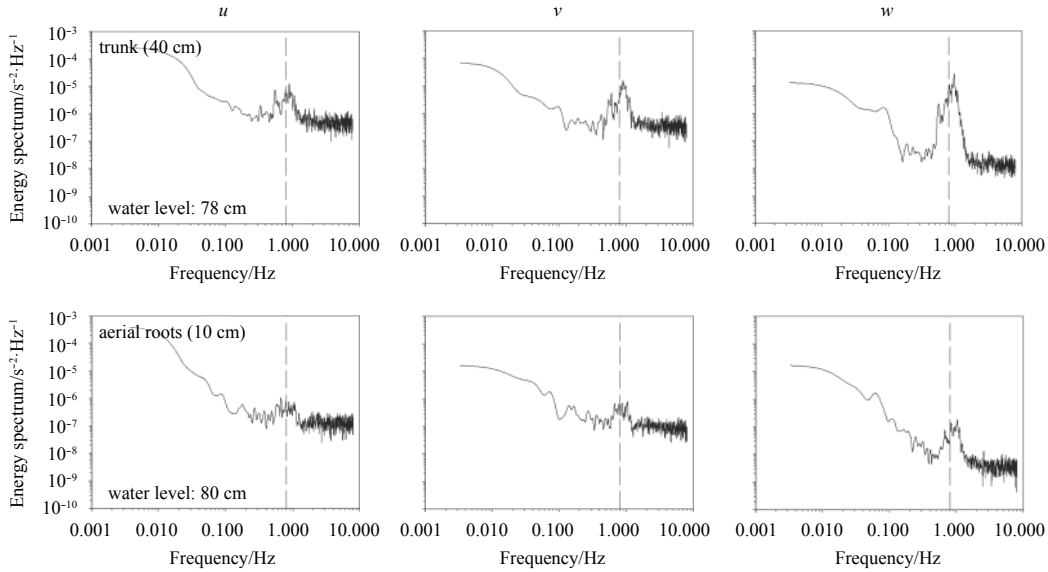

Fig. 7. Energy spectrum plots of the three flow components based on fixed-point measurements at two elevations during the daytime tide.

the half wavelength, which corresponds to the Bragg reflection, is 2.25 m (Guazzelli et al., 1992). The Bragg reflection is similar to the width of the canopy and the space between the mangrove trees; therefore, this peak value may be caused by the natural vibration between the flows and the mangrove trees (Davies et al., 1984).

5 Discussion

5.1 *Flow velocity profile due to the impact of vegetation*

The flow structure over the bare mudflats is consistent with the theory of a turbulent boundary layer, the vertical flow velocity essentially agrees with a semi-logarithmic distribution (Soulsby, 1997), and the overall profile of the flow velocity has a J-shape (Fig. 8a).

When herbaceous plants appear on a tidal flat (such as Spartina) (Fig. 8), the features of the boundary layer at the bottom will change (Leonard and Luther, 1995; Shi et al., 1995; Leonard and Croft, 2006; Neumeier and Amos, 2006); the main variation is the decrease of the flow velocity in the canopy of the plants. Because the biomass of herbaceous plants is denser at the bottom than at the top, the flow velocity increases with the increasing height, but the mean flow velocity generally decreases (Fig. 8b).

Because there is a certain distance between the canopy and the bottom of the mangrove trees, the observed flow velocity feature in the boundary layer at the bottom of the mudflats with mangrove trees has a pattern in which the flow velocity below the canopy decreases as the height increases (Fig. 8c). Previous studies have found that in vegetated tidal flats, the reduction of the flow velocity is mainly caused by the resistance of the plants (Mazda et al., 1997; Furukawa et al., 1997; Nepf, 1999). Flow in the mangroves is affected not only by the bottom of the tidal flat but also by the vertical variation of the biomass of mangrove trees. In this study, we use the horizontal shear stress to estimate

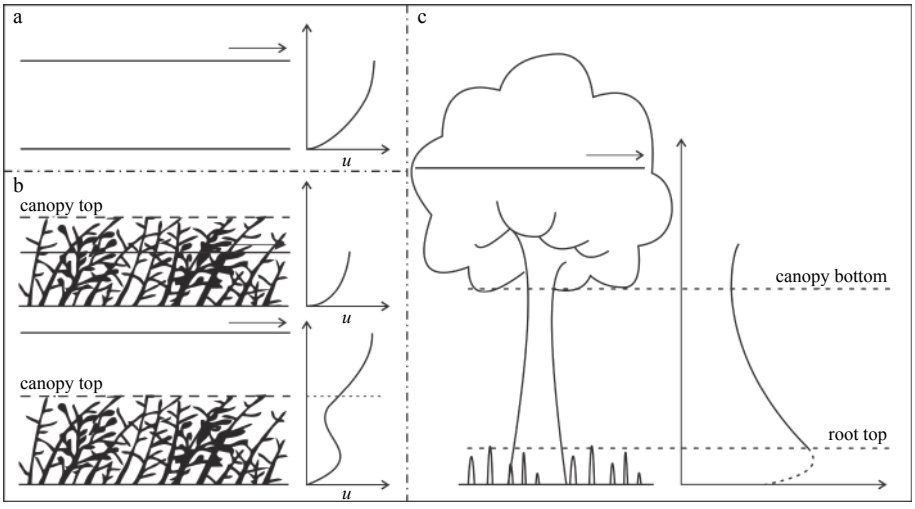

Fig. 8. Comparison of vertical velocity profiles: bare mudflat (a), salt marsh (emergent vegetation and submerged vegetation, adapted from Allen, 2000) (b), and mangroves (c).

the resistance to flow at different heights (Thompson et al., 2003):

$$\tau_{xy} = -\rho\overline{u_t v_t}. \quad (4)$$

The results indicate that from the bottom to the canopy, the shear stress increases from 0.148×10^{-3} to 1.91×10^{-3} N/m^2 (Table 1). The profile of the flow velocity in the mud flats is assumed to follow a semi-logarithmic distribution (Soulsby, 1997); however, the observed profile of the vertical flow velocity shows an inverse logarithmic distribution in the range of the mangroves. The shear stress near the canopy is one order of magnitude higher than that in the near-bottom region, which results in the inverse logarithmic velocity profile shown in this study.

5.2 *Energy dissipation by vegetation*

Compared with studies that have focused on the reduction of the flow velocity caused by vegetation, only limited field observations have been conducted on the energy attenuation within tidal flats with plants. The observations of Leonard and Luther (1995) indicate that the turbulence intensity on sparse *Spartina alterniflora* flats is one order of magnitude lower than that on the bare mudflats and the turbulence intensity of dense *Spartina alterniflora* flats is two orders of magnitude lower than that on the bare mudflats. The *in situ* observations of Neumeier and Amos (2006) in the Ria Formosa lagoon in Europe indicate that in submerged *Spartina*, the turbulent energy tends to be identical in the vertical direction within the canopy of plants; i.e., there is little variation from the bottom to the top. Above the canopy, the turbulence of the water is not affected by the plants, and the turbulent energy increases rapidly. On the bare mudflats, the turbulent energy increases from the bottom to the surface of the water (Soulsby, 1997). According to research results from a laboratory flume, due to the influence of rigid plants, the turbulent energy is lower at the bottom. As the height increases, the energy increases to a maximum on the top interface of the plants and then begins to decrease (López and García, 2001). This is significantly different from the spatial distribution of the turbulent energy for the mangrove trees observed in this study. The flume experiment mainly calculates the turbulent energy based on the vertical transfer of a momentum, and the model considers the plants to be vertically uniform. However, the bottom part of natural mangrove trees contains aerial roots, the middle part is the rigid trunk, and the upper part is the flexible canopy. The turbulence is generated at the interfaces between the trunk and the roots and between the trunk and the canopy. For this specific interface, the vertical transfer of momentum will be intensified, and strong turbulence usually appears, similar to the top interface of herbaceous plants (Neumeier and Amos, 2006). In addition, due to the presence of the root system and plant leaves, some small-scale vortices related to the characteristics of the plant itself could form and increase the turbulence intensity (Nepf, 2012). However, a comparison between a bare mudflat and a mangrove boundary showed that the mangroves generally dissipated turbulence rather than generating more turbulence (Chen et al., 2016).

The energy spectrum within mangrove trees is also different from those in the bare mudflats and salt marshes (Fig. 9). The energy density on the bare mudflats decreases with increasing frequency and follows a power-law pattern (Fig. 9; bare mudflat). The energy spectrum characteristics of a sparse salt marsh and a dense salt marsh are similar to those of a bare mudflat, but the salt marsh's energy density is generally lower than that of the bare mudflat (Fig. 9). The dissipation of a high frequency turbulent energy still follows a power-law behavior with a slope of –5/3

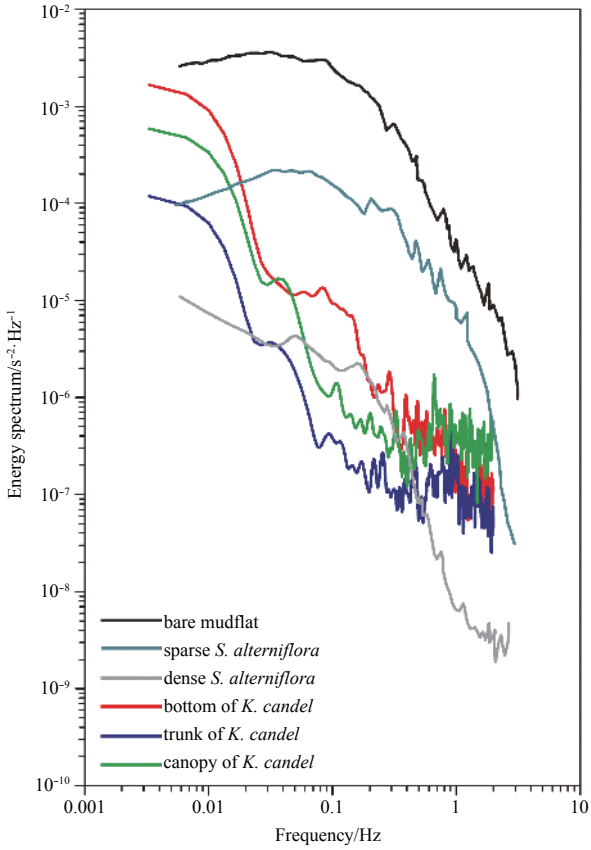

Fig. 9. Comparison of the energy spectrum characteristics of tidal flows within a bare mudflat (Leonard and Luther, 1995), salt marsh (Leonard and Luther, 1995) and mangroves (this study).

(Leonard and Luther, 1995).

In contrast, the energy density distribution in the mangrove trees observed in this study is significantly different from that of the aforementioned three cases when the water level reaches the canopy (Fig. 9). The high-frequency energy density decreases substantially within the trunk and canopy parts, and the slope is much less than –5/3, which indicates that the canopy of the mangrove trees can effectively absorb the high-frequency turbulent energy. However, in the near-bottom part of the mangrove trees, the energy density spectrum follows the –5/3 power law, which indicates that the energy dissipation in this part is different from those in the other two parts. When the water level does not reach the canopy of the mangrove trees, the energy density distribution of the mangrove site is similar to that of a salt marsh and follows a classic power-law dissipation. However, when the water level reaches the canopy, the high-frequency part decreases rapidly, which disrupts the power-law dissipation. In such circumstances, there is an obvious peak at approximately 0.8 Hz in the low-frequency part, which corresponds to a wavelength similar to the canopy width of the mangrove trees and the space between the mangrove trees; this is likely caused by the plant geometry and the spatial arrangement of the trees. This further supports the concept that there is a difference between the canopy and the near-bottom part of the mangrove trees in terms of energy dissipation (James et al., 2006; Chen et al., 2016).

6 Conclusions

In this study, we performed *in situ* observations to investigate

the influences of mangrove trees on the vertical velocity profile, the TKE distribution and the energy spectrum features. The overall findings of this work can be summarized as follows.

(1) We developed an automatic lifting system to observe the vertical velocity profile within a mangrove forest during high water stages. During the spring tides, the flow velocity within the investigated mangroves is low; the flow velocity is less than 4 cm/s throughout the vertical profile. Because the flow in the study area is relatively slow, the turbulence intensity inside the mangrove trees is relatively low.

(2) The observed flow velocity profile in this study is affected by the presence of mangroves. The vertical profile has a pattern in which the flow velocity decreases with increasing height above the bed. Thus, the profile of the vertical flow velocity has an inverse logarithmic distribution. This is because the bottom part of a mangrove tree is composed of sparse pneumatophores, which provide less drag force than the middle part (rigid trunk) and the upper part (canopy). The shear stress near the canopy is estimated to be one order of magnitude higher than that in the bottom part. Thus, the vertical velocity profile is mainly modified by the vertical structure of the mangrove trees.

(3) The vertical structure of the turbulent energy of mangrove trees is also non uniform. The turbulent energy is relatively low in the middle part, but it becomes greater in the upper and lower parts, which results in a C-type distribution. The energy density spectrum indicates a variation that depends on the water level relative to the canopy.

Acknowledgements

We thank Zhenyu Sun from Xiamen University for his support in fieldwork. Thanks extend to the local management office of Ximen Island National Nature Reserve, for the site access.

References

Allen J R L. 2000. Morphodynamics of Holocene salt marshes: a review sketch from the Atlantic and Southern North Sea coasts of Europe. Quaternary Science Reviews, 19(12): 1155–1231, doi: 10.1016/S0277-3791(99)00034-7

Bao T Q. 2011. Effect of mangrove forest structures on wave attenuation in coastal Vietnam. Oceanologia, 53(3): 807–818, doi: 10.5697/oc.53-3.807

Barbier E B, Hacker S D, Kennedy C, et al. 2011. The value of estuarine and coastal ecosystem services. Ecological Monographs, 81(2): 169–193, doi: 10.1890/10-1510.1

Chen Yining, Li Yan, Cai Tinglu, et al. 2016. A comparison of biohydrodynamic interaction within mangrove and saltmarsh boundaries. Earth Surface Processes and Landforms, 41(13): 1967–1979, doi: 10.1002/esp.v41.13

Davies A G, Heathershaw A D. 1984. Surface-wave propagation over sinusoidally varying topography. Journal of Fluid Mechanics, 144: 419–443, doi: 10.1017/S0022112084001671

Furukawa K, Wolanski E, Mueller H. 1997. Currents and sediment transport in mangrove forests. Estuarine, Coastal and Shelf Science, 44(3): 301–310, doi: 10.1006/ecss.1996.0120

Goring D G, Nikora V I. 2002. Despiking acoustic Doppler velocimeter data. Journal of Hydraulic Engineering, 128(1): 117–126, doi: 10.1061/(ASCE)0733-9429(2002)128:1(117)

Guazzelli E, Rey V, Belzons M. 1992. Higher-order Bragg reflection of gravity surface waves by periodic beds. Journal of Fluid Mechanics, 245: 301–317, doi: 10.1017/S0022112092000478

Han Gengchen, Yang Xinmei. 2017. Research and Practice on Regulation and Control Technology of Marine Special Protected Areas (in Chinese). Beijing: China Ocean Press, 161–167

James K R, Haritos N, Ades P K. 2006. Mechanical stability of trees under dynamic loads. American Journal of Botany, 93(10): 1522–1530, doi: 10.3732/ajb.93.10.1522

Leonard L A, Croft A L. 2006. The effect of standing biomass on flow velocity and turbulence in *Spartina alterniflora* canopies. Estuarine, Coastal and Shelf Science, 69(3–4): 325–336

Leonard L A, Luther M E. 1995. Flow hydrodynamics in tidal marsh canopies. Limnology and Oceanography, 40(8): 1474–1484, doi: 10.4319/lo.1995.40.8.1474

López F, García M H. 2001. Mean flow and turbulence structure of open-channel flow through non-emergent vegetation. Journal of Hydraulic Engineering, 127(5): 392–402, doi: 10.1061/(ASCE)0733-9429(2001)127:5(392)

Massel S R, Furukawa K, Brinkman R M. 1999. Surface wave propagation in mangrove forests. Fluid Dynamics Research, 24(4): 219–249, doi: 10.1016/S0169-5983(98)00024-0

Mazda Y, Wolanski E. 2009. Hydrodynamics and modeling of water flow in mangrove areas. In: Gerardo M E, Wolanski E, Cahoon D R, et al., eds. Coastal Wetlands: An Integrated Ecosystem Approach. Amsterdam: Elsevier, 231–261

Mazda Y, Wolanski E, King B, et al. 1997. Drag force due to vegetation in mangrove swamps. Mangroves and Salt Marshes, 1(3): 193–199, doi: 10.1023/A:1009949411068

Middleton G V, Southard J B. 1984. Mechanics of Sediment Movement. 2nd ed. Rhode Island: SEPM

Mitsch W J, Gosselink J G. 2000. The value of wetlands: importance of scale and landscape setting. Ecological Economics, 35(1): 25–33, doi: 10.1016/S0921-8009(00)00165-8

Nepf H M. 1999. Drag, turbulence, and diffusion in flow through emergent vegetation. Water Resources Research, 35(2): 479–489, doi: 10.1029/1998WR900069

Nepf H M. 2012. Flow and transport in regions with aquatic vegetation. Annual Review of Fluid Mechanics, 44(1): 123–142, doi: 10.1146/annurev-fluid-120710-101048

Neumeier U, Amos C L. 2006. The influence of vegetation on turbulence and flow velocities in European salt-marshes. Sedimentology, 53(2): 259–277, doi: 10.1111/sed.2006.53.issue-2

Perillo G M E, Wolanski E, Cahoon D R, et al. 2009. Coastal Wetlands: An Integrated Ecosystem Approach. Oxford, UK: Elsevier

Quartel S, Kroon A, Augustinus P G E F, et al. 2007. Wave attenuation in coastal mangroves in the Red River Delta, Vietnam. Journal of Asian Earth Sciences, 29(4): 576–584, doi: 10.1016/j.jseaes.2006.05.008

Shi Z, Pethick J S, Burd F, et al. 1996. Velocity profiles in a salt marsh canopy. Geo-Marine Letters, 16(4): 319–323, doi: 10.1007/BF01245563

Shi Z, Pethick J S, Pye K. 1995. Flow structure in and above the various heights of a saltmarsh canopy: a laboratory flume study. Journal of Coastal Research, 11(4): 1204–1209

Soulsby R. 1997. Dynamics of Marine Sands: A Manual for Practical Applications. London: Thomas Telford

Thompson C E L, Amos C L, Jones T E R, et al. 2003. The manifestation of fluid-transmitted bed shear stress in a smooth annular flume-a comparison of methods. Journal of Coastal Research, 19(4): 1094–1103